Review on Modeling Development for Multiscale Chemical Reactions Coupled Transport Phenomena in Solid Oxide Fuel Cells

Andersson, Martin; Yuan, Jinliang; Sundén, Bengt

Published in:
Applied Energy

DOI:
10.1016/j.apenergy.2009.11.013

2010

Title: Review on Modeling Development for Multiscale Chemical Reactions Coupled Transport Phenomena in Solid Oxide Fuel Cells

Authors: Martin Andersson* (martin.andersson@energy.lth.se), Jinliang Yuan* (jinliang.yuan@energy.lth.se), Bengt Sundén* (bengt.sunden@energy.lth.se)

*Department of Energy Sciences, Lund University, SE-221 00 Lund, Sweden

Corresponding author: Jinliang Yuan, +46 46 222 4813, Department of Energy Sciences, Lund University, SE-221 00 Lund, Sweden

Abstract

A literature study is performed to compile the state-of-the-art, as well as future potential, in SOFC modeling. Principles behind various transport processes such as mass, heat, momentum and charge as well as for electrochemical and internal reforming reactions are described. A deeper investigation is made to find out potentials and challenges using a multiscale approach to model solid oxide fuel cells (SOFCs) and combine the accuracy at microscale with the calculation speed at macroscale to design SOFCs, based on a clear understanding of transport phenomena, chemical reactions and functional requirements. Suitable methods are studied to model SOFCs covering various length scales. Coupling methods between different approaches and length scales by multiscale models are outlined. Multiscale modeling increases the understanding for detailed transport phenomena, and can be used to make a correct decision on the specific design and control of operating conditions. It is expected that the development and production costs will be decreased and the energy efficiency be increased (reducing running cost) as the understanding of complex physical phenomena increases. It is concluded that the connection between numerical modeling and experiments is too rare and also that material parameters in most cases are valid only for standard materials and not for the actual SOFC component microstructures.

Keywords: SOFC, multiscale modeling, review, chemical reaction, transport phenomena

1 Introduction

Fuel cells directly convert the free energy of a chemical reactant to electrical energy and heat. This is different from a conventional thermal power plant, where the fuel is oxidized in a combustion process combined with a conversion process (thermal-mechanical-electrical energy), that takes place after the combustion [1]. If pure hydrogen is used, no pollution of air and environment occurs at all, because the output from the fuel cells is electricity, heat and water. Fuel cells do not store energy as batteries do [2]. A fuel cell consists of two electrodes: one anode for fuel and one cathode for oxidant. The electrodes are separated by the electrolyte and connected into an electrically conducting circuit. A gas or liquid, with fuel or oxidant, is transported to the electrode, which should be permeable via a porous structure. Unit cells are further organized together into stacks to supply the required electricity [3].

The solid oxide fuel cell (SOFC) electrolyte is non porous ceramic, normally Y_2O_3 stabilized ZrO_2 (YSZ). At an operating temperature between 600-1000 °C, the ceramic electrolyte becomes non-conductive for electrons, but conductive to oxygen ions. Cathodes are mostly made from electronically conducting oxides or mixed electronically conducting and ion-conduction ceramics. The anode consists normally of nickel/yttria stabilized zirconia (Ni/YSZ) cermet. SOFCs can be designed with planar, tubular or monolithic structures. The planar design is normally more compact, compared to the tubular design, i.e., a higher volume of specific power is achieved. Tubular and planar SOFCs can be either electrolyte-, anode-, cathode- or metal- supported. An electrolyte-supported SOFC has thin anode and cathode (~50 μm), and the thickness of the electrolyte is more than 100 μm. This design works preferably at temperatures around 1000 °C. In an electrode-supported SOFC either the anode (anode-supported) or the cathode (cathode-supported) is thick enough to serve as the supporting substrate for cell fabrication, normally between 0.3 and 1.5 mm. The electrolyte is in this configuration very thin, and the operating temperature can be reduced to an intermediate range [4].

The current trend is to decrease the operating temperature. Low temperature (LT)-SOFCs in the range of 300-600 °C is under development, the challenge is to increase the ionic conductivity in the electrolyte. Low temperatures make it possible to use cheaper materials throughout the fuel cell system. An approach with material development on the nanoscale is expected to be very promising [5].

As an alternative to the conventional SOFCs (SOFC-O) with electrolyte of YSZ, the concept of proton ceramic electrolyte (such as $BaCeO_3$ based ceramics) has been developed (SOFC-H). Complete fuel utilization is possible, since the water is produced in the cathode (instead of in the anode) and no dilution of the fuel occurs. Thermodynamic analysis has shown that a higher theoretical efficiency can be reached, compared to conventional SOFC-O [6].

The fuel cell is not a new invention, since the electrochemical process was discovered already in 1838-39. The interest in fuel cells has been growing exponentially, which is evident from the amount of published scientific papers, after year 2000 [7]. Among various types of fuel cells (FCs), the SOFC has attained significant interest due to its high efficiency and low emissions of pollutants to the environment. High temperature operation offers many advantages, such as high electrochemical reaction rate, flexibility of using various fuels and toleration of impurities [8]. Fuel cell systems are still an immature technology in early phases of development, as can be noted due to lack of a dominant design, few commercial systems and a low market demand. The creation of strategic niche markets and search for early market niches are of a vital importance for the further development. It is expected that mass production will start when a dominant design is found, and then production cost will significantly decrease due to the economy of scale [7].

SOFCs can work with a variety of fuels, e.g., hydrogen, carbon monoxide, methane, ammonia and combinations of these [9-10]. Oxygen is reduced in the cathode (eq. (1)). The oxygen ions are transported through the electrolyte, but the electrons are prevented to pass through the electrolyte. The electrochemical reactions (eqs. (2)-(3)) take place at the anodic three-phase boundary (TPB). Methane needs to be reformed (eq. (4)) before the electrochemical reactions [11]. Carbon monoxide can be oxidized in the electrochemical reaction (eq. (3)) but can also react with water (eq. (5)). Ammonia is converted to hydrogen (eq. (6)). The reactions described here are the overall reactions, more detailed reaction mechanisms can be found in [11-12]. Note that methane and ammonia are not participating in the electrochemical reactions at the anodic TPB, methane is catalytically converted, within the anode, into carbon monoxide and hydrogen and ammonia into nitrogen and hydrogen. Hydrogen and carbon monoxide are used as fuel in the electrochemical reactions [10,12].

$$O_2 + 4e^- \Leftrightarrow 2O^{2-} \quad (1)$$

$$H_2 + O^{2-} \Leftrightarrow H_2O + 2e^- \quad (2)$$

$$CO + O^{2-} \Leftrightarrow CO_2 + 2e^- \quad (3)$$

$$CH_4 + H_2O \Leftrightarrow 3H_2 + CO \quad (4)$$

$$CO + H_2O \Leftrightarrow H_2 + CO_2 \quad (5)$$

$$2NH_3 \Leftrightarrow N_2 + 3H_2 \quad (6)$$

A literature review is conducted to find out what methods have been developed to model SOFCs, arranged according to length scales. The mechanisms behind the transport processes within SOFCs are outlined, in terms of momentum-, mass-, heat- and charge transport. Approaches to model electrochemical as well as internal reforming reactions are discussed in detail. Coupling between different methods, length scales and multiscale model integration are outlined. SOFC microscale models correspond in many cases to the atom or molecular level. The Finite Element Method (FEM) and Finite Volume Method (FVM) are used to model SOFCs at the macroscale level. Multiscale modeling is found to be a promising tool for fuel cell research. COMSOL Multiphysics, based on the FEM, as well as FLUENT, based on the FVM, are examples of commercial codes for analysis of coupling different physical models at different scales. Multiscale modeling increases the understanding for detailed transport phenomena, and can be used to make a correct decision on the specific design and control of operating conditions. Note that this paper focuses on phenomena occurring on the component and the cell level, and an introduction to the stack models can be found in [13] and to the system models in [14].

2 Transport phenomena mechanisms

SOFCs can be examined from different points of view: as an electrochemical generator in a viewpoint of electrochemical reactions at continuum level, as a heat and mass exchanger in a perspective of fluid dynamics and transport phenomena, or as a chemical reactor in viewpoints of chemical reactions depending on fuel composition and heat effects associated with the electrochemical conversion [4].

The amount of fuel gases transported to the active surface for the electrochemical reactions are governed by different parameters, such as porous microstructure, gas consumption, pressure gradient between the fuel flow duct and porous anode, and inlet conditions [15]. The gas molecules diffuse to the three phase boundary (TPB), where the electrochemical reactions take place. The supply of reactants can be the rate limiting step, since the gas molecule diffusion coefficient is much smaller than that for ions. The charge transfer chemistry at the interface between the electrolyte and the anode proceeds on the basis of the hydrogen concentration. The hydrogen concentration depends on the transport within the porous anode and the heterogeneous reforming reaction chemistry. The concentration of the fuel gases, CH_4, CO and H_2, decreases along the length of the fuel channel while the concentration increases for H_2O and CO_2. As a result the current density decreases along the fuel channel [16].

Two approaches for defining the electrochemical reactions can be found in the literature, either as source terms in the governing equations [17-18] or as interface conditions defined at the electrode/electrolyte interfaces [19-24]. Selection of either approach affects the momentum-, heat transfer- and mass transport equations. The approach defining interface conditions can be used, because the thickness of the active layer is sufficiently thin, compared to the thickness of the electrode [19-24]. The reason for using an approach where the electrochemical reactions are defined as source terms is that the reaction zone can be spread out into the electrode some distance away from the electrode/electrolyte interface [17].

For steady state problems, the boundary conditions can be defined with two types of spatial conditions, either as a "*Dirichlet boundary condition*", where the generic value at the boundary is a known and constant value or as a "*Neuman boundary condition*", where the derivates of the generic variable are known [25].

2.1 Mass transport

Mass transport in the electrodes occurs in the gas phase, integrated with the chemical reforming reactions at the solid active surface. The electrodes are porous and mass transfer is dominated by gas diffusion [16]. The interconnect can be assumed to be impermeable for gases. Electron transport effect on the mass transfer needs to be considered since the current is collected [4].

Fick's model is the simplest diffusion model used for dilute or binary systems [26]. In the literature the Stefan-Maxwell model is commonly used to calculate the diffusion in a multi-component system. In some references the Stefan-Maxwell model is combined with the Knudsen diffusion term (frequently called

the Dusty-Gas model or extended Stefan-Maxwell equation) [18,20,27-30], to predict the collision effects between the gas molecules and the solid porous material. In other models this effect is neglected [16].

Dusty-Gas model (DGM), Ficks model (FM) and Stefan-Maxwell model (SMM) are developed in [19], in order to predict the concentration over-potential inside an SOFC anode. DGM and FM consider molecular diffusion, Knudsen diffusion and the effect of a finite pressure gradient. The flux ratio in DGM depends on the square-root of the gas molecular weight, but it does not for FM. Explicit analytical expressions describing fluxes can be used in FM. The SMM can be seen as a simpler model since it does not consider the Knudsen diffusion. DGM is the most appropriate model for H_2-H_2O and CO-CO_2 system. However, it is only used when the operating current density is high. Ni *et al.* [12,31] studied the effect of micro-structural grading on SOFC performance with a DGM to analyze the coupled phenomena of mass transfer and electrochemical reactions in the SOFC electrodes.

To account for the increased diffusion length due to the tortuous paths of real pores in the porous materials, different approaches can be found in the literature [25]:

$$D_{ij,eff} = \varphi^t \cdot D_{ij} \tag{7}$$

$$D_{ij,eff} = \frac{\varphi}{t} \cdot D_{ij} \tag{8}$$

where D_{ij} is the Maxwell-Stefan binary diffusion coefficient, $D_{ij,eff}$ the effective Maxwell-Stefan binary diffusion coefficient in the porous medium, φ the porosity and t the tortuosity. Similar expressions can be found for molecular diffusion coefficients in porous materials [29,30]. Tortuosities up to the range of 10-17 can be found in the literature. These values are too high considering that the range for porous sintered ceramics is reported to be 2-10 [29].

The Maxwell-Stefan equation can be formulated as [32]:

$$\nabla\left(-\rho \cdot w_i \sum D_{ij,eff} \cdot \nabla x_j + \left(x_j - w_j\right)\frac{\nabla p}{p} \cdot \mathrm{u} - D_i^T \cdot \frac{\nabla T}{T} \right) + \rho \cdot \mathrm{u} \cdot \nabla w_j = S_i \tag{9}$$

$$x_j = \frac{w_j}{M_j} \cdot M \tag{10}$$

$$\sum_{i=1}^{n} w_i = 1 \tag{11}$$

where w is the mass fraction, x the mole fraction, D_i^T the thermal diffusion coefficient and S_i the source term due to chemical reactions. The effective diffusion coefficient ($D_{ij,eff}$) equals the molecular diffusion coefficient (D_{ij}) in the gas channels.

Mass or molar fractions need, for the inlet fuel- and air flows, to be defined at the cell level. The outlet conditions are usually defined as convective fluxes. The effects on mass transport from the electrochemical reactions are either defined as source terms in the governing equations or as interface conditions, as discussed previously [33].

For instance, Andersson [33] has developed a model considering fluid flow, mass- and heat transfer for a single cell IT-SOFC. The mole fraction of oxygen (Figure 1) decreases along the flow direction in the air channel and the cathode. There is a concentration difference in the y-direction as well, that forces the flow towards the cathode/electrolyte interface. However, it is hard to recognize in the air channel as the cell length is 400 times bigger than the air channel height.

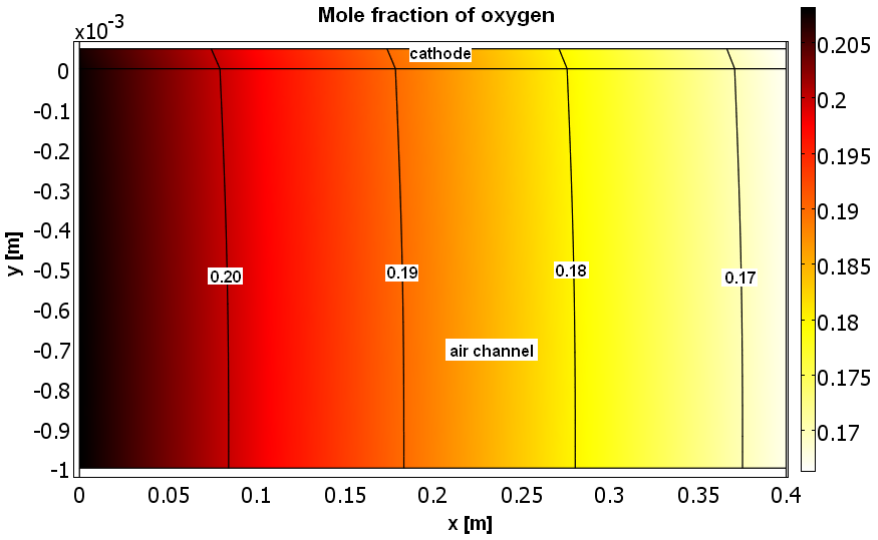

Figure 1: Mole fraction of oxygen in the air channel and cathode for a single cell IT-SOFC [33].

2.1.1 Knudsen diffusion

For the porous material, molecular diffusion is predominant for the case with large pores, whose size is much bigger than the free path of the diffusion gas molecules [18], i.e., the Stefan-Maxwell model describes the transport processes with a satisfactory accuracy. The Knudsen diffusion is used when the pores are small in comparison to the mean free path of the gas. In this case, molecules collide more often with the pore walls than with other molecules. The Knudsen diffusion coefficient can be calculated using a kinetic theory that relates the diameter of the pore and the mean free path of the gas according to [30]:

$$D_k = \frac{\mathrm{u} \cdot r'}{6} \tag{12}$$

where D_k is the Knudsen diffusion coefficient, r' is the average pore radius and u is the velocity of the gas molecules. If the pores are straight and circular, the diffusion coefficient of the component i is [30]:

$$D_{ik} = 97.0 \cdot r' \cdot \sqrt{\frac{T}{M_i}} \tag{13}$$

where D_{ik} is the Knudsen diffusion coefficient for molecule i, T the temperature and M_i the molecular weight. To calculate the average pore radius (r'), the surface area of the porous solid and the porosity are used [30]:

$$r' = \frac{2 \cdot \varphi}{\mathrm{SA} \cdot \rho_B} \tag{14}$$

where SA is the surface area of the porous solid and ρ_B the bulk density of the solid particle. It is possible to account for the tortuous path of the molecule, by calculating the effective Knudsen diffusion coefficient [30]:

$$D_{ik,eff} = D_{ik} \cdot \left(\frac{\varphi}{t} \right) \tag{15}$$

where $D_{ik,eff}$ is the effective Knudsen diffusion coefficient. Molecular diffusion and Knudsen diffusion may appear at the same time and can be calculated as [26,30]:

$$\frac{1}{D_{i,eff}} = \frac{1}{D_{ij,eff}} + \frac{1}{D_{ik,eff}} \tag{16}$$

2.2 Momentum transport

The fuel cell manifolds should be designed with the aim to achieve uniform fluid distribution between different unit cells and a stable stack operation. The flow field in a unit cell may be divided into three parts, inlet manifold, cell gas channels (fuel and air) and outlet manifold. The inlet manifold for a single cell is a part of the stack inlet manifold, the air (or fuel) is directed into the single cell and the excess is transported to the next cells. For a stack with a given number of single cells, the geometric parameters that are influential to the stack flow uniformity are: the height of the repeating unit cell, the height and length of the gas channels, the inlet manifold width and the outlet manifold width [34].

The effects of the geometric parameters on the stack flow uniformity are normally understandable in terms of their effects on the relative dominances between the pressure changes in the gas channels and manifolds. According to a study in [34], the fuel flow distribution is more uniform than the air flow distribution for a given stack, due to the fact that the fuel flow velocity is small or in the laminar region, with a small pressure change in the manifold. The results also show that the flow distribution for stacks with a large number of cells can be far from ideal conditions. It is revealed that the ratio between inlet and outlet manifold widths is a key parameter for the flow distribution, and the optimal ratio increases with the number of cells in the stack.

The gases flow inside the fuel cell components, such as in the air and fuel channels and to the porous electrodes. The physics of laminar and turbulent incompressible flow are well described by the Navier-Stokes equations. It is common practice to assume laminar flow for fuel cell gas channels due to the low velocities, which decreases the computational cost significantly [25]. The Darcy equation describes the balance in the porous electrodes between the force from the pressure gradient and the frictional resistance from the solid material. It should be noted that the Darcy equation expresses the flow in the porous structure well away from the walls. A traditional modeling approach for such a system consists of solving the Darcy's equation in the porous medium and the Navier-Stokes equations in the channels separately. The problem with such an approach is to define interfacial conditions at the interface between the two domains. It is hard to define this tangential velocity component. To avoid this problem the Darcy-Brinkman equation is introduced and solved for the gas flow in the fuel and air channels and in the porous media (electrodes) [20,32,35].

The Darcy-Brinkman equation (eq. (17)) is transformed into the standard Navier-Stokes equation when ($\kappa \to \infty$) and (ε_p=1), and into the Darcy equation as ($Da \to 0$). *Da* is the Darcy number. The derivation of the Navier-Stokes equation and Darcy equation from Darcy-Brinkman equation can be found in [35].

$$\left(\frac{\mu}{\kappa} + \rho \cdot \nabla \mathrm{u}\right) \cdot \mathrm{u} - \nabla\left[-p + \frac{1}{\varphi}\left\{\mathbf{T} - \left(\lambda - \kappa_{dv}\right)\left(\nabla \mathrm{u}\right)\right\}\right] = \mathbf{F} \tag{17}$$

where $\mathbf{F}$ is the volume force vector, κ the permeability of the porous medium, φ the porosity, μ the dynamic viscosity, u the velocity vector and $\mathbf{T}$ the viscous stress tensor $\left(\mathbf{T} = v\left(\nabla \mathrm{u} + \left(\nabla \mathrm{u}\right)^T\right)\right)$. κ_{dv} is the deviation from thermodynamic equilibrium. When this term is zero, the fluid particles are in equilibrium with their surroundings. λ is the second viscosity and is, for gases, normally assumed as: λ=-2/3 μ [36].

When a single cell is modeled, a velocity (profile) is defined at the air- and fuel channel inlets (frequently as a laminar flow profile) and pressure at the air- and fuel channel outlets. The effects from the electrochemical reactions are either defined as source terms in the governing equations or as interface conditions as discussed previously [33,37].

2.3 Heat transport

The heat transfer inside SOFCs includes various aspects such as convective heat transfer between the solid surfaces and the gas streams, conductive heat transfer in solid and porous structures. Heat generation occurs due to the electrochemical reactions at TPB between the electrolyte and electrodes [38], the current flow (ohmic polarization) and the internal reforming reactions of carbon monoxide at the porous anode and in the fuel channel [39]. The steam reforming reaction of methane in the porous anode is endothermic, and heat is then consumed [39]. Accurate temperature prediction distribution within SOFCs is essential for predicting and optimizing the overall cell performance as well as avoiding thermo-mechanical degradation [40]. Most of the heat within SOFCs is generated near the electrode/electrolyte interface and is dissipated by: (1) conduction in the solid matrix, (2) heat transfer from the solid to the gas phase by convection within the pores and (3) advection of the gas through the micro-pores to the flow channel [40].

Effective transport parameters for the porous material need to be calculated when a local temperature equilibrium (LTE) approach (assumes the same temperature for gas- and solid phase) is used. The thermal conductivity (k_{eff}) and specific heat ($c_{p,eff}$) can be specified as [18]:

$$k_{eff} = \varphi \cdot k_f + (1-\varphi) \cdot k_s \tag{18}$$

$$c_{p,eff} = \varphi \cdot c_{p,f} + (1-\varphi) \cdot c_{p,s} \tag{19}$$

where φ is the porosity, *eff* means effective, *s* solid and *f* fluid (gas) phase. The temperature distribution can be predicted by [32]:

$$\nabla(-k_{eff} \cdot \nabla T) = Q - \rho_{eff} \cdot c_{p,eff} \cdot \mathrm{u} \cdot \nabla T \tag{20}$$

where T is the temperature (same temperature is assumed for solid- and gas phase), and Q the source term (due to the chemical- and the electrochemical reactions).

2.3.1 Local temperature non-equilibrium (LTNE) approach

A very common method in SOFC modeling is to employ LTE [18,26,40]. However, some typical conditions found in the porous SOFC electrodes bring this assumption into question: (1) very low Reynolds number flow, (2) presence of volumetric heat generation and (3) large difference in thermal conductivities between the gas- and solid phases. A local temperature non-equilibrium (LTNE) approach is developed in [40] to predict the temperature difference between the solid- and gas phases within the porous electrodes. Heat is (according to the LTNE approach) transferred between the phases at the solid material surfaces in the porous electrodes. The general heat conduction equation is used to calculate the temperature distribution for the solid matrix in the porous electrodes [32]:

$$\nabla(-k_s \cdot \nabla T_s) = Q_s \tag{21}$$

where k_s is the thermal conductivity of the solid, T_s the temperature in the solid phase and Q_s the heat source (heat transfer between the solid- and gas phases, the heat generation due to the ohmic polarization and due to the internal reforming reactions). The heat generation due to electrochemical reactions, concentration polarization and activation polarization can be defined either as a source term or as an interface condition. Note that part of the heat generation/consumption enters into the solid phase and the remaining part to the gas phase. Knowledge about this ratio is still pore. The temperature distribution for the gas mixtures in the fuel and air channels, and in the porous electrodes can be defined as [32]:

$$\nabla(-k_g \cdot \nabla T_g) = Q_g - \rho_g \cdot c_{p,g} \cdot \mathrm{u} \cdot \nabla T_g \tag{22}$$

where $c_{p,g}$ is the gas phase heat capacity, T_g the gas temperature and Q_g the heat transfer between the gas- and solid phases and the heat generation that occurs in the gas phase. Because the Reynolds number is very low inside the porous electrodes, the heat transfer coefficient, $h_{s,g,por}$ (when spherical particles are assumed in the porous electrodes) can be calculated as [40]:

$$h_{s,g,por} = \frac{2 \cdot k_g}{d_p} \tag{23}$$

where d_p is the electrode particle diameter and k_g the gas conductivity. The heat transfer between the gas- and solid phase depends on the temperature difference and the particle surface area as [41]:

$$Q_g = h_v \cdot (T_g - T_s) = SA \cdot h_{s,g,por} \cdot (T_g - T_s) \tag{24}$$

where h_v is the volume heat transfer coefficient and *SA* the surface area ratio.

Most cell level models define the temperature at the air and fuel channel inlets and convective flux at the outlets. The boundaries at the top and bottom of the cells are (for a cell model) normally defined by symmetries, when the cell is assumed to be surrounded by other similar cells with the same temperature distribution [33].

For example, Andersson [33] uses a LTNE approach to calculate the temperature distribution for a single cell IT-SOFC. The temperature increases along the x-direction (the main flow direction), as seen in Figure 2. The temperature difference in the y-direction inside the air channel occurs because the convective heat flux is bigger in the air channel (compared to the fuel channel) due to the relatively larger gas flow rate. It is revealed that the temperature difference between the phases is less than 1K for the studied case (not shown here).

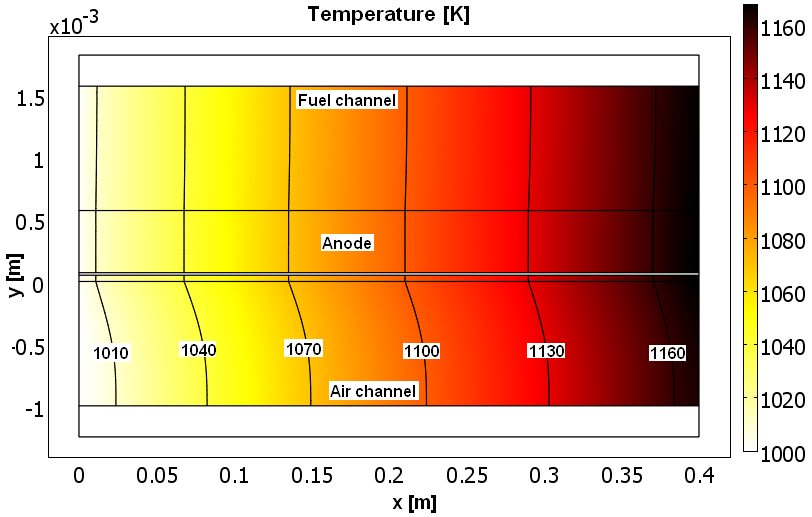

Figure 2: Temperature for the gas phase in a single cell IT-SOFC [33].

2.3.2 Thermal radiation

SOFCs are operating at a high temperature and thus thermal radiation should be involved for an accurate heat balance. Heat exchange between the surfaces of the air and fuel channels, radiation between the surfaces of the channels and flowing gases (especially water and carbon dioxide) and radiation heat loss from the stack to the environment should be taken into account for effective thermal management of the fuel cell stack. The thermal radiation between the surfaces may be calculated as [42]:

$$q_i = \sum_{j=1}^{n} A_i F_{ij} k' \left(T_i^4 - T_j^4 \right) \tag{25}$$

where the radiation leaves surface i as a result of its interaction with surface j, T is the temperature (in Kelvin), k' is the Bolzmann constant and F is the view factor. The net rate between the channel surfaces (assumed to have blackbody conditions) and the channel gases can be expressed as [42]:

$$q_{net} = A_s k' \left(\varepsilon_g T_g^4 - \alpha_g T_s^4 \right) \tag{26}$$

where A is the active surface area, ε the emissivity and α the absorptivity.

2.4 Charge transport

The SOFC electrolyte has two functions: to transport oxide ions from the electrolyte to the anode and to block electron flow from the anode to the cathode [11]. The flow of electronic charges through external circuit balances the flow of the ionic charge through the electrolyte and electrical power is produced [43]. This transport can be described by considering the ion transport from the conservation of charge as [26]:

$$\nabla \cdot i = 0 = \nabla \cdot i_{io} + \nabla \cdot i_{el} \tag{27}$$

$$-i_{io} = \nabla \cdot i_{el} \tag{28}$$

$$i_{io} = -\sigma_{io}^{eff} \nabla \phi_{io} \tag{29}$$

Eq. (29) is Ohm's law, i_{io} and i_{el} are charge fluxes for ions and electrons, respectively, and ϕ_{io} is the ionic potential in the electrolyte. The interfaces/boundaries can be defined as electric potential (V=V_0), electric isolation (n•i=0) or ground conditions (V=0). The effects of the electrochemical reactions are either defined as source terms in the governing equations or as interface conditions at the electrolyte/electrode interface, as previously discussed [32]. Bessler *et al.* [37] assume that the electrode component has a constant electric potential.

The Nernst potential is usually calculated as the sum of the potential differences across the anode and cathode [26]:

$$E = \Delta\phi_a + \Delta\phi_c \tag{30}$$

where E is the reversible electrochemical cell voltage and $ø$ the charge potential.

2.5 Interaction issues

The mass-, heat-, momentum- and charge transport and the chemical reactions are dependent on each other. The fluid properties and the flow field (momentum transport) depend on the temperature and the species concentrations. The (electro-) chemical reaction rates depend on temperature, species concentrations and available surface areas for catalytical reactions. The chemical reactions generate and consume heat, i.e., the temperature distribution depends on the chemical reaction rates, as well as on the solid and the gas properties (for example the heat capacity and the conductivity). All these dependences require that the governing equations are solved coupled [1].

3 Micro catalytic reaction mechanisms

3.1 Electrochemical reactions

Electrochemical reactions occur at the TPB, i.e., the region where the electrode, electrolyte and gas phase meet. Ions migrate in the ionic phase, conduction of electrons occurs in the electronic phase and transport of gas molecules takes place in the porous part of the electrodes. A larger TPB area gives more reaction sites (= lower activation polarization in the electrodes) [16]. Note that the TPB needs to be connected to the rest of the structure, i.e., the pores need to be connected through the surrounding pore network to the fuel/air stream, the nickel phase must be connected to the current collector and the YSZ phase to the bulk YSZ electrolyte [29].

The total pressure is lower close to TPB, compared to other parts of the cathode due to the consumption of oxygen molecules at TPBs. This gradient makes the transport of oxygen from the channel towards the electrolyte easier. The TPB area in the electrode depends on the particle diameter. A reduction of the particle diameter increases the TPB area, at the same time the Knudsen diffusivity and the flow permeability are reduced. In [16] it is found that most of the electrochemical reaction occurs within 10 μm (from the electrolyte interface) for the anode and 50 μm for the cathode when the mean particle diameter is 1 μm [16].

At the interface between the electrode and electrolyte the Bulter-Volmer equation can be used to calculate the volumetric current density [30]:

$$i = i_0 \left\{ \exp\left(\beta \cdot \frac{n_e \cdot \mathrm{F} \cdot \eta_{act,e}}{\mathrm{R} \cdot T} \right) - \exp\left(-(1-\beta) \frac{n_e \cdot \mathrm{F} \cdot \eta_{act,e}}{\mathrm{R} \cdot T} \right) \right\} \tag{31}$$

where F is the Faraday constant, R the ideal gas constant and β the transfer coefficient, usually assumed to be 0.5. The Butler-Volmer equation can often be expressed as [30]:

$$i = 2 \cdot i_0 \cdot \sinh\left(\frac{n_e \cdot \mathrm{F} \cdot \eta_{act,e}}{2 \cdot \mathrm{R} \cdot T} \right) \tag{32}$$

$$\eta_{act,e} = \frac{2 \cdot \mathrm{R} \cdot T}{n_e \cdot \mathrm{F}} \sinh^{-1}\left(\frac{i_e}{2 \cdot i_{0,e}}\right) \tag{33}$$

$$i_0 = \frac{R \cdot T}{n_e \cdot F} k''_e \cdot \exp\left(\frac{-E_e}{\mathrm{R} \cdot T}\right) \tag{34}$$

where i_o is the exchange current density, k'' the pre-exponential factor and E the activation energy.

The charge transfer processes are ones of the least understood aspects of fuel cell chemistry [29,44]. It is expected that understanding the mechanism of the surface reactions that occur close to the anode TPB is important for the future advances of the SOFC development [44]. Most models in the literature assume a single global charge transfer reaction, leading to the Bulter-Volmer equation (eq. (31)). Adsorption/desorption, surface diffusion, the formation of hydroxyl and a charge transfer reaction are all found to be feasible rate-limiting steps in an SOFC (anode) model [29].

A five elementary reaction mechanism for the electrochemical reactions used by Lee *et al.* [29], among others, reads:

$$H_2(g) + 2(Ni) \Leftrightarrow 2H(Ni) \tag{35}$$

$$H(Ni) + O_2(YSZ) \Leftrightarrow (Ni) + OH^-(YSZ) + e^-(Ni) \tag{36}$$

$$H(Ni) + OH^-(YSZ) \Leftrightarrow (Ni) + H_2O(YSZ) + e^-(Ni) \tag{37}$$

$$H_2O(YSZ) \Leftrightarrow H_2O(g) + (YSZ) \tag{38}$$

$$O_0^X(YSZ) + (YSZ) \Leftrightarrow O^{2-}(YSZ) + V_0^{\bullet\bullet}(YSZ) \tag{39}$$

Hydrogen is assumed to be adsorbed only at the nickel *(Ni)* surface and other surface species at the electrolyte surface *(YSZ)*. Interactions between (1) adsorbed atomic hydrogen *H(Ni)*, an empty surface site (Ni) and an electron $e^-(Ni)$, (2) a lattice oxygen O_0^X(YSZ) and an oxygen vacancy, $V_0^{\bullet\bullet}(YSZ)$ within the YSZ electrolyte, and (3) hydroxyl ion $OH^-(YSZ)$, water $H_2O(YSZ)$, oxygen ion $O^{2-}(YSZ)$ and empty *YSZ* sites are considered in this reaction mechanism (eqs. (35)-(39)). The expression for the exchange current density depends on the assumption of which equation is the rate limiting one, as shown in Table 1. Note that different expressions can be obtained, based on the dependence on the partial pressure of the product and reactants, anodic or cathodic reaction coefficient (k_a or k_c) and the equilibrium constants (K) for the respective reactions. Determination of the actual rate-limiting reactions among eqs. (35)-(38) requires a very careful analysis and fitting of experimental data to the different theoretical derivations. Also the anodic and cathodic charge-transfer coefficients in the Butler-Volmer equation depends on the assumption of the rate-limiting equations. The hydrogen adsorption rate can be described as: $i^*_{H_2} \cdot p_{H_2}$, where $i^*_{H_2}$ can be seen as an adjustable parameter (connected to the exchange current density) to match the experimentally observed performance [29].

Table 1: Exchange current density in Bulter-Volmer equation when assuming different rate-limiting conditions for the anode electrochemical reactions [29].

Rate limiting reaction	Exchange current density (i_0)	Hydrogen adsorption ($i^*_{H_2} \cdot p_{H_2}$)
Eq. (35)	$i_0 = i^*_{H_2}\left(p_{H_2}\right)$	$2Fl_{TPB}\frac{S_i^0}{\sqrt{2\pi RTM_{H_2}}} \cdot p_{H_2}$
Eq. (36)	$i_0 = i^*_{H_2}\frac{p_{H_2O}^{1/4}\left(K_{30}p_{H_2}\right)^{1/4}}{1+\left(K_{30}p_{H_2}\right)^{1/2}}$	$\frac{2Fl_{TPB}K_{34}^{1/4}k_{31,a}^{3/4}k_{31,c}^{1/4}}{\left(K_{32}K_{33}\right)^{1/4}} \cdot p_{H_2}$
Eq. (37)	$i_0 = i^*_{H_2}\frac{p_{H_2O}^{3/4}\left(K_{30}p_{H_2}\right)^{1/4}}{1+\left(K_{30}p_{H_2}\right)^{1/2}}$	$2Fl_{TPB}k_{32c}\left(K_{32}K_{31}\right)^{1/4}\left(\frac{K_{34}}{K_{33}}\right)^{3/4} \cdot p_{H_2}$
Eq. (38)	$i_0 = i^*_{H_2}\left(p_{H_2O}\right)$	$2Fl_{TPB}K_{34}k_{33b} \cdot p_{H_2}$

Vogler *et al.* [44] studied the electrochemical hydrogen oxidation reaction at nickel/YSZ anodes and considered eq. (35)-(39) but also the YSZ surface reaction between water and oxygen ions, Ni surface reaction for water and hydroxyl ions, and five additional charge transfer reactions. Their computational model is based on elementary physics and chemical processes (without the assumption of a specific rate-determining step). Models and experiments are compared to determine the anode performance and to estimate the pre-exponential factors and the activation energies. Only the forward-rate coefficients from the experimental and literature data are used and then the reverse-rate constants are calculated according to thermodynamic consistency. Seven possible different combinations of one or two elementary charge transfer reactions are investigated and compared to the experimental data. It is found that the hydrogen spillover mechanisms (eq. (37) together with eq. (40)) have best agreement with the experimental data. The calculated activation energy (using experimental data) is higher than expected. This may be explained by an unfavorable geometry at atomic scale.

$$H(Ni) + O^{2-}(YSZ) \Leftrightarrow (Ni) + OH^{-}(YSZ) + e^{-}(Ni) \tag{40}$$

A high TPB length (or area) is required for high electrochemical performance, and of crucial importance for the fuel cell performance. Janardhanan *et al.* [45] concluded that the maximum volume specific TPB length is achieved at 50 % porosity (while other parameters are fixed). A mathematical model is developed in [45] based on porosity, particle diameter and volume fraction of the ionic- and electronic phase. The calculation can be based on both uniform and non-uniform particle size distributions.

Asinari *et al.* [46] uses the lattice Boltzmann method to construct a 3D microscopic topology, where the TPB area is calculated. Both the electron and the ion dynamics are included in the numerical model. In order to realize an electrochemical reaction the electron conducting cell (EEC) must be in contact with the electron sink, i.e., at least one connection path must exist between the EEC in question and the collection grid.

Martinez and Brouwer [47] have developed a Monte Carlo percolation model to be able to characterize the factors controlling the TPB formation within an SOFC electrode. The model considers ionic and electronic conductor, gas phase percolation, competition between percolation of gas and electronically conducting phases. It is found that physical processes such as sorbate transport significantly affect the TPB formation. It is also concluded that the TPB formation is most effective when the electronic volume fraction is quite low.

The contribution to the gas species distributions (in mol/(m^{2}s)) by the electrochemical reactions is given as [25,27,48]:

$$r_{H_2} = \frac{-i}{2 \cdot \mathrm{F}} \tag{41}$$

$$r_{H_2O} = \frac{i}{2 \cdot \mathrm{F}} \tag{42}$$

$$r_{O_2} = \frac{-i}{4 \cdot \mathrm{F}} \tag{43}$$

where i is the current density and F the Faraday constant.

3.2 Internal reforming reactions

Internal reforming reactions inside SOFC porous anodes enable the conversion of hydrocarbon fuels (and water) into hydrogen and carbon monoxide, and further carbon monoxide (and water) to hydrogen. The heat, needed by the steam reforming reaction, is generated in the electrochemical reactions at the active surface (TPB) between the porous anode/electrolyte and cathode/electrolyte. A good heat transfer (in terms of short heat transfer distance between heat generation and consumption within the cell) can be achieved and the conversion efficiency is increased. Hydrogen and carbon monoxide can be oxidized as soon as they are produced by the reforming reactions, and steam produced by the electrochemical reaction (eq. (2)) can be used in the reforming reactions (eqs. (4)-(5)) [15,49].

The steam reforming of hydrocarbon fuels (eqs. (4)-(5)) could either take place before the fuel cell stack (in an external pre-reformer) or inside the cell in the anode (internal reforming). A pre-reformer needs extra added steam, since it can not use the steam generated in the electrochemical reactions. The internal

steam reforming reaction takes place over ceramic-supported nickel catalysts and decreases the requirement for cell cooling (less surplus of air). Less steam is needed for the reforming reactions and finally it offers advantages with respect to the capital cost. Up to half of the heat produced by the oxidation reaction (exothermic) could be "consumed" by the steam reforming process. This would improve the system electrical efficiency [39].

The probability for carbon depositions depends on the steam/methane ratio. It has been well established that the key reactions occur over a surface layer of nickel atoms. If a layer of carbon is allowed to build up and attach to a nickel crystallite rapid catalyst breakdown can occur, due to the graphite formation. It should be noted that hydrocarbons with a longer coal chain than methane have a higher propensity for carbon deposition. To avoid the carbon deposition inside the SOFC anode pre-reforming have to be carried out before the fuel enters into the cell at a lower temperature at which carbon deposition does not occur [50].

In a conventional (high temperature (HT)) SOFC (with nickel content of about 50 vol.% and operating temperature about 1000 °C) the endothermic reaction is very fast. This can result in a temperature drop at the inlet of the stack. The temperature gradient results in thermal tensions, which in the worst case causes mechanical failure of the cells [39]. The problem of the tensions and big temperature gradients close to the inlet could be solved with different approaches:

(1) Lowering the operating temperature to an intermediate range to reduce the steam reforming reaction rates [51].

(2) Recycling a part of the anode gas to obtain a dilution of the fuel. The rate of reforming reactions decreases, due to decrease in fuel concentration. A 50 percent recycling results in sufficient steam for the reforming reactions and the cost for a separate water supply is saved [39].

(3) The anode material can be designed with the aim of a decreased steam reforming activity. Until now these new SOFC materials (such as iron or copper) have too low electronic conductivity to meet the real world requirements. When nickel is replaced during the fabrication process with for example iron, a less catalytic active anode regarding the reforming activity is constructed. This is in the short term a promising method, and this approach is based on well-established production processes. Other researches replace nickel with copper and the same effect has been reached [39].

The reforming reactions occur in the porous anode. The reaction rates can be described with simplified global expressions (3.2.1) or detailed expressions for surface chemical reactions (3.2.2). Some models in literature are compared in terms of internal reforming reaction mechanisms and involved gas species, as in Table 2. It is found that comparison with experimental data is rare. Most of the models [6,23,52-55] use an equilibrium approach both for the water-gas shift reaction and steam reforming reaction. For the steam reforming reaction a comparison of the kinetic expression with different dependences of water and methane is presented in this table. It is common to use an inlet concentration considering 30-% pre-reformed natural gas, which is also specified as IEA (International Energy Agency) conditions [6,23,54-55]. The ratio of water to methane is varied, in [53], to study the effect of gradual vs. direct internal reforming reactions.

Table 2. Comparison of models considering internal reforming reactions.

	Sanchez *et al.* [52]	Klein *et al.* [53]	Janardhanen Deutschmann [27]	Nagel *et al.* [54]	Wang *et al.* [55]	Lehnert *et al.* [23]	Aguiar *et al.* [51]	Ni *et al.* [6]
Fuel (inlet vol-%)								
CH_4	0.09	*	0.970	0.171	0.171	0.171	0.280	0.171
CO	0.07	n/a	0	0.029	0.029	0.029	0.005	0.029
CO_2	0.22	n/a	0	0.044	0.044	0.044	0.030	0.044
H_2	0.28	n/a	0	0.263	0.263	0.263	0.120	0.263
H_2O	0.34	*	0.030	0.493	0.493	0.493	0.565	0.493
Equations								
Equilibrium reactions	X	X		X	X	X		X
Surface reactions			X					
m (eq. (44)) ¤	1/0.85	n/a	n/a	1/0.85 /1	n/a	n/a	1/1/0.85/1.4	n/a
n (eq. (44)) ¤	0/-0.35	n/a	n/a	0/-0.35/ 1	n/a	n/a	-1.25/0/-0.35/0.8	n/a
Comparison with exp. data								
Yes			X					
No	X	X		X	X	X	X	X

* The ratio of water to methane (x_{H2O}/x_{CH4}) is varied between 0.01 and 1.

¤ A comparison study between different equations for reaction rates, in the reference, is made when more than one value is presented [51-52,54].

3.2.1 Global reforming reaction kinetics

Methane can be converted to hydrogen and carbon monoxide inside the porous anode by the catalytic steam reforming. Carbon monoxide reacts further (inside the anode as well in the fuel channel) with steam to produce hydrogen and carbon dioxide according to the water-gas shift reaction [24,56]. The overall reactions can be written as eqs. (4)-(5). Hydrogen reacts with oxygen ions at the anodic TPB and generates steam. As hydrogen is consumed and steam is generated, the water-gas shift reaction proceeds towards the right, i.e., more hydrogen is produced. The catalytic reforming reactions occurs at the surface of the porous structure inside the anode [55].

Several kinetic expressions considering the steam reforming reaction are developed in the literature. The reaction order varies significantly between the models, in terms of orders of methane and water (*m* and *n* in eq. (44)), see Table 2 for typical values. The reaction order of methane (*m*) varies between 0.85 and 1.4. The highest difference in reaction orders is found for water (*n*), both negative and positive values exist, however, it has been shown that all these findings could be correct for the chosen operating conditions of the experiments. Small steam-to-carbon (SC) ratio gives positive reaction order of water. SC in the order of 2 yields the reaction orders of water close to zero, and high SC gives negative values [54]. Experimental work has shown that it is possible to change the steam reforming reaction orders by modifying the anode, for example *m* increased from 0.85 to 1.4 and *n* decreased from -0,35 to -0,8 when basic compounds are added in Ni-YSZ anode [51]. As seen in Table 2, comparison with experimental data is rare, but it is worth while to note that the reaction orders (*m* and *n*) usually originate from fitting experimental data to a kinetic expression.

$$r_r = k \cdot p_{CH_4}^{m} \cdot p_{H_2O}^{n} \cdot \exp\left(\frac{-E_a}{\mathrm{R} \cdot T}\right) \tag{44}$$

where r_r is the reaction rate of steam reforming reaction (in mol/s/m), p the partial pressure (in bar), R the ideal gas constant and T the temperature. The reaction rate is converted to mol/s/m^2 after multiplying the reaction rate (mol/s/m) with the surface area ratio (SA). The kinetic expression (eq. (44) can be compared to the equilibrium approach (eq. (45)) [54].

$$r_{r,eq} = k \cdot p_{CH_4} \cdot p_{H_2O} \cdot \left(1 - \frac{p_{CO} \cdot p_{H_2}^{3}}{K_{e,STR} \cdot p_{CH_4} \cdot p_{H_2O}}\right) \tag{45}$$

where K_e is the equilibrium constant. The reaction orders in eq. (45) are the same as the molar proportions for the respective gas species in the global chemical reaction (1 for both methane and water for the forward reaction, and 3 for hydrogen and 1 for carbon monoxide for the backward reaction).

Different approaches for defining the water-gas shift reaction (eq. (5)) can be found in literature: (1) Global reaction mechanism that considers reaction in the anode only [6,18]. (2) Global reaction mechanism that considers reaction in the anode and in the fuel channel [53,57]. (3) A more advanced reaction mechanism that includes catalytic surface reaction kinetics for steam reforming, water-gas shift reaction and the Boudouard mechanism can be found in [27,58]. It is frequently stated in literature [52-53,57] that the water-gas shift reaction should be considered to be in (or very close to) equilibrium state. When the equilibrium is assumed the reaction velocity can be expressed with an equilibrium-limited shift reaction rate expression, first order in carbon monoxide as [55]:

$$r_s = k_s \cdot p_{CO} \cdot \left(1 - \frac{p_{CO_2} \cdot p_{H_2}}{K_{e,s} \cdot p_{CO} \cdot p_{H_2O}}\right) \tag{46}$$

where r_s is the reaction velocity of the water-gas shift reaction, k_s the pre-exponential factor, p_i partial pressure for the respective species and $K_{e,s}$ the temperature dependent equilibrium constant [55].

The concentration of the different gases in the anode (the steam reforming and the water-gas shift reactions) and fuel channel (the water-gas shift reaction) is changing as the above described reactions proceed:

$$r_{CH_4} = -r_r \tag{47}$$

$$r_{H_2} = 3 \cdot r_r + r_s \tag{48}$$

$$r_{CO} = r_r - r_s \tag{49}$$

$$r_{CO_2} = r_s \tag{50}$$

$$r_{H_2O} = -r_r - r_s \tag{51}$$

where r_i is the reaction rate of species i. The catalytic steam reforming rate is expressed by r_r and the water-gas shift reaction rate by r_s.

Andersson [33] uses a global approach to calculate internal reforming reactions for a single cell SOFC. The gas-phase temperature within the cell is presented in Figure 3. The steam reforming reaction reduces the temperature close to the fuel channel inlet. The temperature is slightly lower on the air side (compared to the fuel side), due to a higher air flow rate. The initial temperature decrease is found to be 15 K in the anode, compared to 14 K in the cathode, 13 K in the fuel channel and 11 K in the air channel. For the case with higher operating temperature a higher reforming reaction rate is expected and also the temperature close to the inlet decreases faster. The mole fraction distribution of methane can be seen in Figure 4. The concentration difference in the y-direction is due to the consumption of methane in the porous structure. Methane diffuses from the channel towards the porous anode. Note that the fuel channel length is 100 times bigger than the channel height.

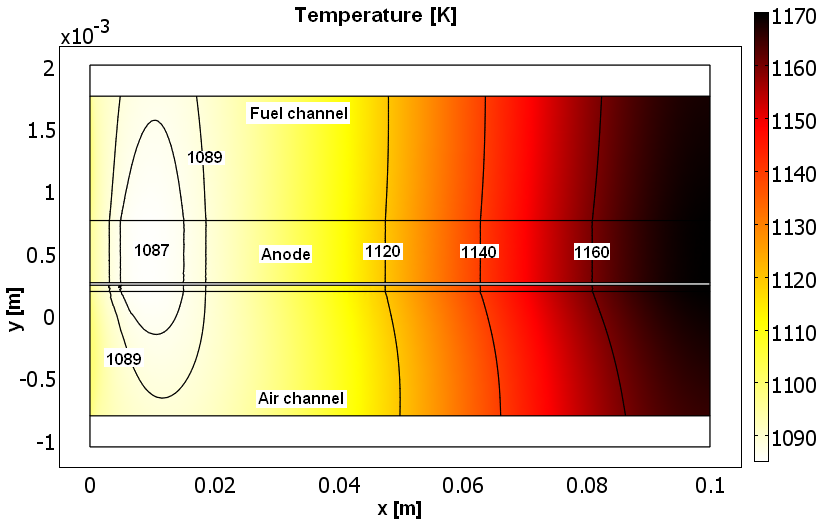

Figure 3: Temperature distribution within the single cell (in the gas phase) when a global approach for internal reforming reactions is employed [33].

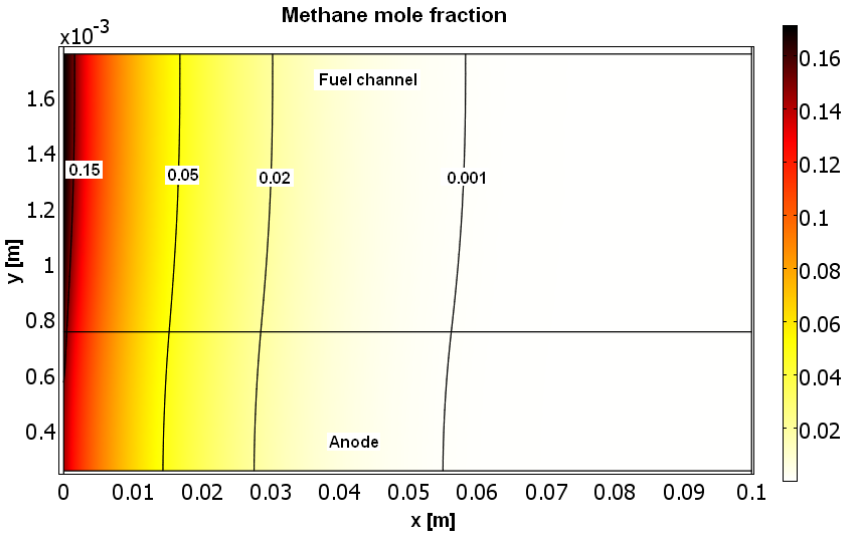

Figure 4: The mole fraction of methane within the anode and fuel channel in Andersson's model [33].

3.2.2 Elementary surface reaction kinetics

Elementary-kinetic electrochemical modeling of SOFC electrodes is strongly connected to the heterogeneous catalysis and the surface chemistry (as shown in Figs. 5-6). Note that information considering the surface coverages are not available when the global approach is applied. Both for the anode and cathode there is (within the literature) a disagreement considering the involved reaction pathways, rate-limiting steps and intermediate species [37,59]. Elementary-kinetic models are normally limited to only the electroactive region, and couplings to transport models are still rare. The electroactive species occurring in the charge transfer reactions are surface-adsorbed intermediates. The surface coverage can be calculated with for example a mean-field approach, where it is assumed that the surface state can be described with average quantities, such as surface coverage, thermodynamic and kinetic adsorbate properties. The composition (segregation phenomena and impurities) and the detailed surface structure (steps, edges and terraces), occurring on the atomic scale, are then not further resolved, when using the mean-field approach. The surface concentration of the different species is normalized to the total concentration of available surface sites, yielding the dimensionless coverage. The surface species are coupled to the gas-phase species via desorption and adsorption reactions, and to bulk-phase species via surface/bulk exchange reactions. The surface species are also participating in the reactions among themselves [37].

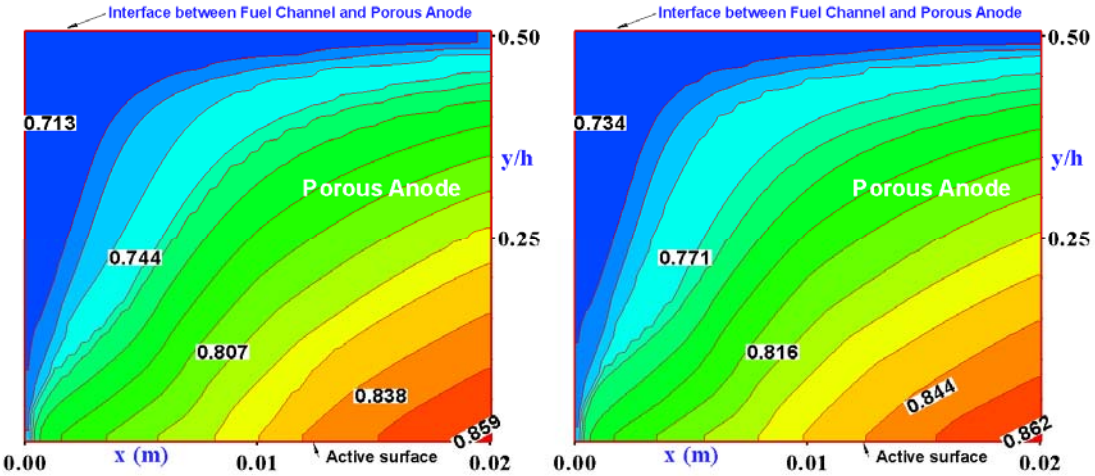

Figure 5: Fraction of Ni_s (empty catalytic sites) at 700°C (left side) and 900°C (right side) along main flow direction of an IT-SOFC anode [60].

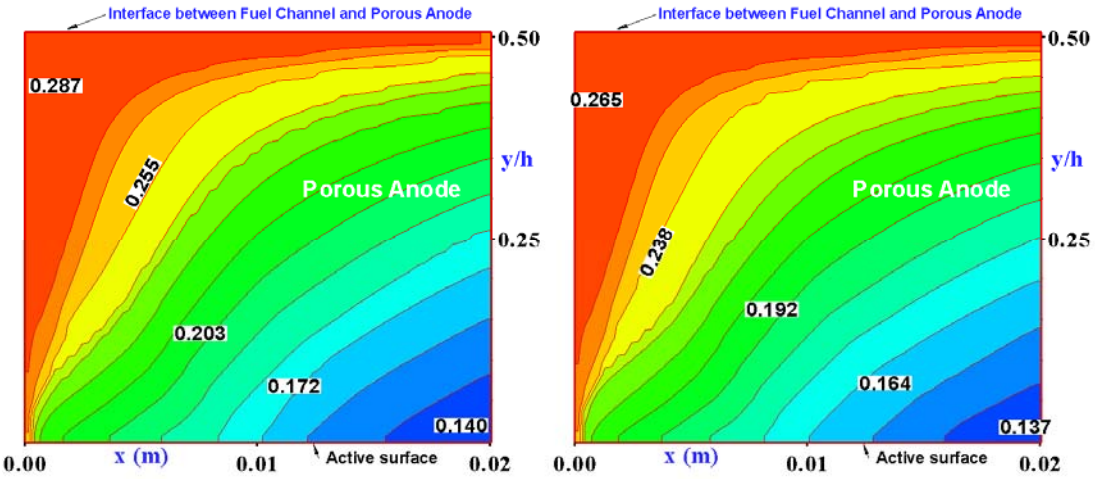

Figure 6: Surface coverage of H_s (hydrogen bound to the catalytic sites) at 700°C (left side) and 900°C (right side) along main flow direction of an IT-SOFC anode [60].

An SOFC anode is normally fabricated as a porous metal-ceramic composite, where the gas, ceramic and metal phases occupy roughly 30 percent of the volume each, the characteristic pore dimensions are in the order of 1 µm [61]. Knowledge of the catalytic reaction mechanism considering reforming of hydrocarbons is counted as a key importance for designing an anode material with a high efficiency and a long life length [62].

Janardhanan and Deutschmann [63] have developed a multi-step heterogeneous reaction mechanism for Ni catalysts. The mechanism consists of 42 reactions, 6 gas-phase species and 12 surface adsorbed species. The mechanism is elementary in nature and covers the global aspects of the reforming, the water-gas shift and the Bouduard reactions. Most of the expressions are expressed in Arrhenius rate form and are dependent on the surface coverage.

Hofmann *et al.* [58] compare the heterogeneous reaction mechanism (HCR) from [48] with a simplified approach, where the methane reforming is described according to a global kinetic approach and the water-gas shift reaction in equilibrium. The HCR model can be used to calculate the catalytic surface coverage. It is concluded that the HCR predicts a less steep methane consumption along the flow channel. Slower methane conversion means less hydrogen available throughout the cell. Also the temperature distribution is significantly affected by the steam reforming reaction, with a flatter temperature gradient for the HCR.

4 Multiscale SOFC modeling development

4.1 Micro-, meso- and macroscale approaches

An SOFC can be described by different length scales: system scale (~10^2 m), component scale (~10^1 m), material aspect at the fuel cell/constituent (~10^{-2} m), flow/diffusion morphologies (~10^{-3} m), material structure/interface (~10^{-6} m, Monte Carlo (MC)- and Continuum Methods (CM) in Fig. 7), and functional material levels (~10^{-9} m, Density Functional Theory (DFT) and Molecular Dynamics (MD) in Fig. 7). Not only proper length scales are needed to describe various parts of an SOFC, also different time scales need to be considered. Cell charging and cathode gas thermal diffusion are in 10^{-3} s, convective transport is in 10^{-1}s, cell heating and anode streamwise thermal diffusion are in 10^3 s and cathode streamwise thermal diffusion is in 10^4 s [8]. A general relation between time- and length scales with proper modeling methods can be seen in Figure 7, DFT and MD corresponds to the microscale, MC and CM to the mesoscale and methods with a length scales bigger than 10 µm (for example Finite Element Method (FEM) and Finite Volume Method (FVM)) to the macroscale. There are two basic approaches for interaction between the different modeling methods (i.e., multiscale modeling): (1) hierarchical methods and (2) hybrid or concurrent methods [64]. These approaches are further described in chapter 4.1.4.

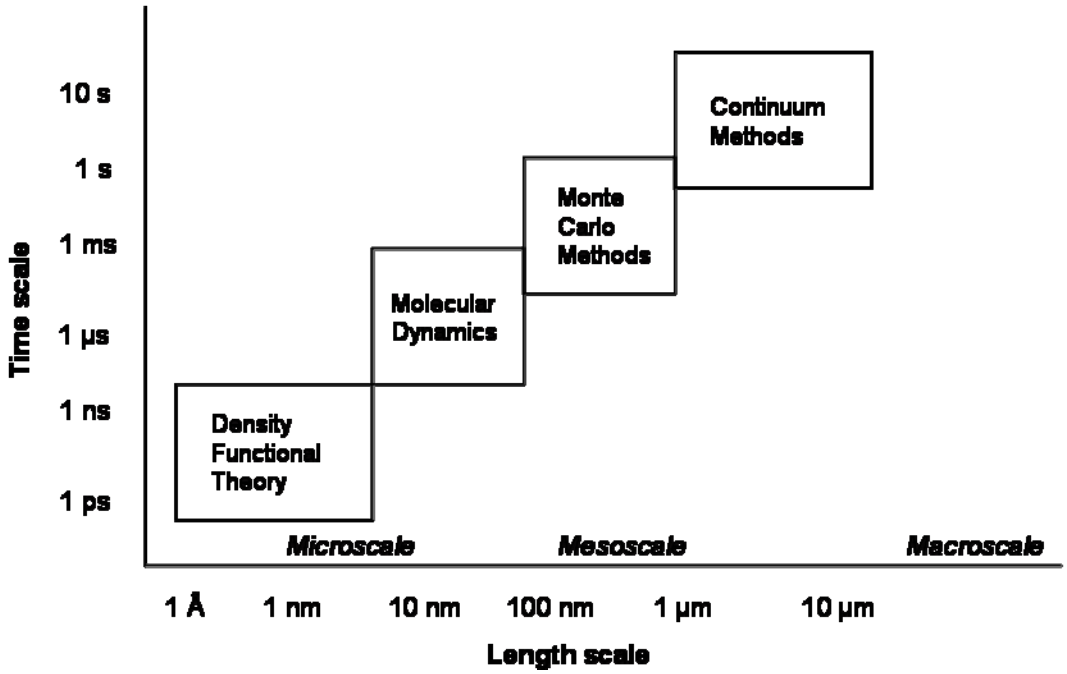

Figure 7: Characteristic time and length scales for various methods [64].

Research of the physical phenomena is based on different levels of scales: micro-, meso- and macroscales. The microscale model corresponds in many cases to the atom or molecular level as thermo- or fluid dynamics and detailed chemical reactions are studied. The microscale does not need to be as small as the size of the molecules. A mesoscale model corresponds to a larger scale than a particle but a smaller one than the facility or the global flow field. Macroscale models match to the global flow field. Microscale modeling is in general more related to theoretical knowledge compared to macroscale modeling that is more related to empirical data. Empirical parameters for macroscale models could be based on the results from micro- or mesoscale models [12].

Instantaneous flow around individual moving particles can be calculated in microscale models. Flows corresponding to calculation cells, larger than particles but smaller than global flow fields, are calculated with mesoscale models. Trajectories of individual particles are calculated with particle motion equations for microscale modeling. The flow field is in mesoscale modeling divided into a number of small cells, but not as small as the particle size [12].

Different methods have been developed to describe different scales. Methods that can be used for SOFC modeling are listed in Table 3, based on micro-, meso- and macroscales.

Table 3: Computational methods arranged after scales [12-15,17,36,64-72].

Microscale	Mesoscale	Macroscale
Density Functional Theory (DFT)	Monte Carlo (MC)	Finite Element Method (FEM)
Quantum Chemistry (QC)	Brownian Dynamics (BD)	Finite Volume Method (FVM)
Lattice-Boltzmann Method (LBM)	Dissipative Particle Dynamics (DPD)	Finite Difference Method (FDM)
Molecular Dynamics (MD)		Spectral Methods (SM)
Mechanistic Models (MM)		

4.1.1 SOFC modeling at microscale

Frayret *et al.* [65] simulated microscopic aspects of oxygen diffusion in ceria-based materials in the ionic conductor with the DFT. This methodology is a good tool to study the connection between dopant ionic radius and diffusion at the atomistic scale. DFT is an “ab inito” method where the material properties are described by solutions of the Schrödinger equation. DFT models have a characteristic length scale of Å – nm and a time scale of ps – ns.

Cheng *et al.* [66] simulated the oxygen ion-hoping phenomenon inside a YSZ electrolyte with MD. MD can be used to model grain boundary structure, specific heat capacity and molecular structure. Systems up to 10^5 atoms and a time scale of the order of ten ns can be modeled [67].

The Lattice-Boltzmann Method (LBM) is used to model mass transport of gases inside the porous anode of an SOFC. The porous structure is based on SEM (scanning electron microscope) images, which are converted to digital form. Advantages of the LBM model are that a detailed analysis of mass transfer can be carried out for the actual anode microstructure; this means that tortuosity is not used as a fitting parameter. LBM approach is according to an investigation in [68] accurate enough to model concentration polarization in 2D. By changing the number of void spaces present in the solid matrix the porosity in the LBM is varied.

More detailed information is needed about the kinetic, thermodynamic, and transport data of species and reactions, particular for the YSZ surface but also for other parts of the cell. This is achievable either with experiments from the surface science or with microscale theoretical approach, such as quantum chemical calculations with DFT and molecular dynamics calculations [44].

4.1.2 SOFC modeling at mesoscale

Modak and Lusk [67] applied kinetic MC to simulate the open-circuit voltage and electrical double layers of a doped electrolyte. Discrete time increments of various size are used to capture diffusion or adsorption in a single step. The physical property data generated by QC and MD can be utilized in the KMC model. Monte Carlo methods have a characteristic length scale of 100 nm – μm and a time scale of ms – s [15].

Huang *et al.* [69] employed COMSOL Multiphysics to model the multiphysics processes in the SOFC cathode-electrolyte interface considering the geometry and detailed distribution of the pores and the ionic conducting phase. The charge transfer rate, electron- and ion conduction are governed in a modeling domain extracted from actual materials encountered in the application. Note that FEM is developed for phenomena occurring in the macroscale. However Huang and coauthors are solving cathode electrochemical processes at mesoscale with COMSOL Multiphysics.

4.1.3 SOFC modeling at macroscale

Cheng *et al.* [66] used the FEM and the commercial software COMSOL Multiphysics to solve the flow equations for macroscopic transport phenomena. Navier-Stokes equations are used to describe the flow conditions in the air and fuel channels and the Darcy law describes the flow conditions in the porous layer. FEM has a characteristic time scale of 1 s and above [65].

A clear relationship between the underlying physical conditions and numerical algorithm has made the FVM a popular method for commercial codes such as PHOENICS, FLUENT, CFX and STAR-CD [36]. Pasaogullari and Wang [70] as well as Autossier *et al.* [71] used FLUENT to solve the equations of momentum, mass, energy, multicomponent species and electrochemical kinetics for an SOFC. Hussain *et al.* [17] employed the FVM to model the transport of multi-component species inside porous SOFC anodes.

Continuum electrochemical models are commonly used in many modeling studies, where the electrical current density, the cell voltage and the heat production are considered. The output voltage is normally expressed as the difference of the open circuit voltage and the polarizations due to the electrical current generation. Continuum electrochemistry models can be used to determine effects of various designs and operating parameters on the generated power, maximum cell temperature, fuel conversion efficiency, stresses caused by temperature gradients and the effects of thermal expansions. The performance of a particular electrode under different operating conditions can be calculated, but sufficient information on how an electrode with different microstructure will perform can not be calculated with the macroscale models. Chemical reactions and species transport characteristics (within the electrode) are affected by the micro-structural parameters. Oxygen ion diffusion and surface diffusions are dependent on the available geometric paths through the structure. The reactive surface availability decides the surface chemical reaction rate. It can be concluded that the ability to model fuel cell characteristics at the microscale level is needed for the electrode design and optimization [72].

4.1.4 SOFC modeling integration issues

Multi-physical problems can often be described with a set of partial differential equations at different length scales. The coupled partial differential equations can be solved simultaneously in physical domains for corresponding physical phenomena. Fuel cell operation depends on complex interaction between multi-physics such as multi-phase fluid flow, mass transport, heat transfer and (electro-) chemical reactions [73]. Two basic integration approaches can be found: hierarchical method, and hybrid and cocurrent method. The hierarchical modeling starts at higher resolution (smaller scale) and properties are extracted and used as input to the next level method. The hierarchical methods are today the most developed methods for

multiscale modeling [65]. Three different methods are used for hybrid approaches to describe various regions of the material with the appropriate time and length scale resolutions. The hybrid methods that permit cocurrent simulations are promising for the future development, since only one calculation needs to be performed, however, it requires more computational power compared to the hierarchical methods [65].

As an example a general hybrid molecular-continuum strategy, i.e., the point-wise coupling methodology (PWC) was presented in [74]. The solution in the entire domain is advanced through the continuum solver and the atomistic models are utilized to: (1) calculate transport properties (such as viscosity for the non-Newtonian fluids and thermal conductivity), (2) provide accurate boundary condition (such as temperature, slip velocity and tangential stress) and (3) substitute constitutive relations for the pressure among others. The MD solver is occupied to calculate macroscopic quantities at selected points in time and space for the prevailing continuum conditions. The transport of information from the molecular to the continuum model is less complicated compared to the opposite direction, however it is crucial for the accuracy and efficiency of the hybrid scheme. The calculation of the macroscopic variables are performed through averaging the corresponding microscopic properties. The PWC effectively avoids performing MC simulations for nearly identical continuum states, meaning a significant reduction in computational time [74].

The particle size in SOFCs is in the sub-micron scale, and the TPBs are in nanoscale. The morphology and properties of these scales are important for the performance of the fuel cell, since they control how much of the Gibbs free energy being available. It means that the sciences at nanoscale are critical to the performance at a system-scale. A robust design and multi-scale analysis should consider those nano-details as well as macro system level [75].

Khaleel *et al.* [72] developed a multiscale approach, where the microscale electrochemistry model (Lattice-Boltzmann algorithm) calculates the performance of the porous electrode material based on material structure at the microstructure level, distribution of reaction surfaces, and transport of oxygen ions through the material. The microscale electrochemistry modeling is used to calculate the overall fuel cell current-voltage relation, which is then used as input to the macroscale calculations (MARC software), where the current density, cell voltage and heat production are calculated.

Bove *et al.* [76] established a macroscale black-box model, using equations that are generally used for microscale models. The main problem with this approach is that the gas composition variation along the flow direction is neglected, the effect of fuel utilization variation can not be estimated and the cell voltage is underestimated. The advantages is that the calculations are less time consuming compared to microscale modeling, and contains more information describing microscale phenomena compared to other macroscale models.

Cheng *et al.* [66] and Pasaogullari and Wang [70] introduced multiscale-concepts; however, they did not mention how the different scales interact with each other. It is frequently stated in the literature that data or property constants can be obtained from smaller scale and then used in a model made at a larger scale. However, information about the construction of this coupling is rare [27,64-65].

4.2 Validation

The numerical results of a computation are only an approximation of the real world conditions and considering that convergence is not sufficient, validation is a necessary step in the development of computational models [25,77]. A range of validity can be established between the developed model and experimental data. Models are usually validated by adjusting estimated physical prosperities values to reach certain agreement [78]. For example adjusting the reaction orders of methane and water in the methane steam reforming reaction according to experimental data is very common.

Microscale approaches, such as Lattice Boltzamann (LB) method can be used to model multi-component gas transport in SOFCs. The diffusive flow in the porous electrodes can then be simulated without any empirical modification of diffusion coefficients, such as medium porosity and tortuosity. Validation of these microscale models are not required [79].

Tortuosity is an important parameter for characterization of fluid flow through porous media in many macroscale models. It is normally considered as a geometric parameter, however, it was originally introduced as a kinematic property, equal to the relative average length of the flow path of a fluid particle from one side of a porous structure to the other side. If a suitable model is developed for the porous medium, then the tortuosity becomes a geometric property. Frequently in the literature tortuosity is treated as a fitting property (used for validation purposes), i.e., the tortuosity should then not be seen as a kinematic- or geometric property [46].

Nicotella *et al.* [80] has developed a model considering mass and charge transport and electrochemical reactions in porous composite cathodes. A validation is performed to compare the experimental data on polarization resistance obtained by impedance spectroscopy on cathodes of different

thicknesses with the simulations. It is concluded that the developed model can replicate the experimental results concerning the dependence of the polarization resistance on the cathode thicknesses, because non-uniform morphological properties are taken into account.

Peksen *et al.* [81] has developed a computational model (based on FVM) for SOFC pre-reformer considering fluid flow, heat transfer, chemical reacting species transport. Surface temperature measurements and species gas compositions are used for validation of the 3D model. Also experimental validation is performed using thermocouples and gas chromatography.

Suwanwarangkul *et al.* [19] modeled transport phenomena inside SOFC anodes. Fick's- Stefan-Maxwell- and Dusty-Gas models were compared. Experimental data from literature were used to compare the calculated concentration overpotential for H_2-H_2O-Ar and CO-CO_2 systems.

4.3 State-of-the-art in multiscale SOFC modeling

Mathematical models are central tools in examining and understanding effects of various operating parameters and designs, as well as promoting the SOFC development. Results from modeling can be used to select optimal operating conditions and to optimize the design. Numerical results obtained from commercial softwares show acceptable accuracy if compared with experimental data as well other modeling predictions [4].

The current state-of-the-art in SOFC modeling is to use computational fluid dynamics (CFD) to solve the transport equations and couple the solution to an electrochemical model. Some models found in the literature are compared in terms of methodology for the modeling, see Table 4. Most of the investigated models [15,17,20,22,24-26] use the finite volume method (FVM) for solving the governing equations. Most authors [15,17,22,24-26,33,82] include a parameter study to test their models, but comparison with experimental data is rare. Regarding the flow configuration co-, counter- as well as cross flow can be found in the literature. Note that it is not relevant to compare flow configurations for models at the component level.

Most authors [15,20,22,2482] do not include material characteristics that are dependent on the temperature. However, refs [15,17,33] define the conductivity as temperature dependent, while the other material characteristic parameters are still defined at one temperature only. All investigated models include governing equations for mass transport, most of them [15,20,24-26,33, 82] for momentum transport, some of them for energy [15,20,26,33] and ionic transport [17,22,24-26]. Pramuanjaroenkij *et al.* [26] included simultaneously the governing equations for mass-, energy-, momentum-, and ionic transport. Models are developed with different aims at component, cell or stack level, and calculations considering entire fuel cells system can also be found in the literature [83], however, is not reviewed in this study. Steady-state conditions are applied in a majority of the models developed so far [19].

The fuel cell is considered as a black box in zero-dimensional modeling. The principles of thermodynamics and electrochemistry are used to find output parameters such as cell efficiency, cell voltage and power output. 1-D modeling can be used to model co- and counter-flow, variation of temperature and concentrations along the flow direction may be studied. There are several sections possible for a 2-D cross-section, and the connection between interconnect and electrode is normally neglected in 2-D modeling. 3-D modeling is needed to acquire detailed knowledge of SOFC performance [42].

Table 4. Comparison of SOFC models.

	Pramuanjaroenkij *et al.* [26]	Hussain *et al.* [17]	Yuan Sundén [15]	Yakabe *et al.* [24]	Haberman Young. [20]	Tseronis *et al.* [82]	Tseronis *et al.* [22]	Andersson [33]
Dimensions								
0-D								
1-D		X				X		
2-D	X					X	X	X
3-D			X	X	X			
Discretization method								
FDM								
FVM	X	X	X	X	X		X	
FEM						X		X
Level of modeling								
Component		X	X	X		X	X	
Cell	X			X				X
Stack					½			
System								
Comparison with exp. data								
Yes				X			X	
No	X	X	X		X	X		X
Governing equations								
Mass	X	X	X	X	X	X	X	X
Energy	X		X		X			X
Momentum	X		X	X	X	X		X
Ionic/electronic	X	X		X			X	
Flow configuration								
Co	X	n/a	n/a			n/a	n/a	X
Counter		n/a	n/a	X		n/a	n/a	X
Cross		n/a	n/a		X	n/a	n/a	
Material char. T dep.								
Yes	σ	σ					σ	
No			X	X	X	X	X	
Parameter study								
Yes	X	X	X	X		X	X	X
No					X			

Most of the studies use only common SOFC material in their modeling, new studies are definitely needed to compare alternative materials, to assess the effect of material on efficiency, degradation etc. Many thermal models consider the cell level only and assume the cell boundaries to be insulated. Stack or system level models should be developed further. Electrochemical modeling considering microstructure geometry and material properties is so far rare in the literature.

It is common to assume that the current density is uniform over the entire electrode, note that this is basically only valid as long as the gas concentration is uniform along the flow channel. The total pressure gradient inside the anode is normally assumed to be neglible. This is correct for a very short cell and when only hydrogen and carbon monoxide is used as fuel, because no net change in the number of moles occur in the gas phase [19].

4.3.1 How far can SOFC modeling reach?

There are still unresolved issues in fuel cell modeling. The exchange current density is used to calculate the activation polarization and it depends on the catalyst for the electrochemical reactions. One problem is that the data in literature is not identical or well explained. Further study of the mechanisms behind the activation polarization is important for the further development [78].

The macroscale modeling have gained a lot of success during the last years in understanding complex phenomena occurring during FC operation and it has been possible to improve the FC design. However the microstructure of the porous electrodes is normally not included in the model. Porosity and tortuosity are, for macroscale models, normally treated as fitting parameters. The difficulty is that these parameters are used to compensate for inaccurate modeling of several phenomena. It has also been shown that different porous microstructure can be characterized with the same porosity, but different hydraulic characteristics, i.e., phenomena at the microscale are not described well by macroscale parameters. One way to overcome these limitations is to apply LBM to simulate gas flow in porous media. It should be noted that LBMs do not require pressure-velocity decoupling or solution of a large system of algebraic equations [46]. Fuel cell

modeling can be significantly improved if submodels being not too expensive (in computational time) are included in a general model [78].

A challenge for the future is to develop approaches for multiscale multiphysics modeling considering coupling of fluid flow, heat transfer, species transport, electrochemical kinetics and also reforming kinetics (when hydrocarbon fuels are used). It has been found that the reaction kinetics for the reforming reactions requires rigorous studies, several heterogeneous reaction mechanisms are developed. However, they did not match each other very well [78].

A grand challenge for future SOFC modeling development is the concept of an inverse coupled multiphysics modeling, where the nano-structured material design is calculated from the defined system requirements, instead of material and other engineering specifications. The activation- and diffusion related polarization losses depend strongly on the nano-structure of the cathode and anode materials, and are good examples for application of this potential approach [75].

5 Conclusions

The fuel cell is not a new invention, the principle dates back to 1838. However, the fuel cell technology is approaching the commercial phase, the potential for the future is enormous and fuel cells can be key components in a future sustainable energy system. To achieve this, the production cost must be decreased and the life time must be increased. One way to decrease the operating cost and also increase the life time is to increase the understanding of multiscale transport- and reaction mechanism within the cell. Fuel cell operation depends on complex interaction between multi-physics such as fluid flow, mass and heat transfer and (electro-) chemical reactions at various scales. Coupling of these multiscale phenomena, i.e., multiscale modeling is promising for future fuel cell research. Micro- and macroscale physical phenomena and chemical reactions could be solved together.

Future models need to go down in scale, to specify where the electrochemical and internal reforming reaction occurs, i.e., where heat is released. Validation with experimental data is still too rare, and the quality of the models will be increased by doing this. Detailed analysis of mass transport phenomena with electrochemical processes, velocity, temperature distributions and the microstructure of component material properties need to be integrated for a performance analysis and efficiency optimization.

A challenge faced is to further develop multiscale models for fuel cell designs. They can provide a clear understanding of operating conditions, transport and reaction phenomena at the microscale connected to, e.g., conditions in the air and fuel channels at the macroscale. It is possible to couple different physical models, for example models at the microscale describing transport phenomena inside an anode with a macroscale model describing the entire fuel cell. Use of multiscale modeling in fuel cell research will lead to an increased power density and also to a decreased cost for development and production, and increased energy efficiency etc.

6 Nomenclature

A	active surface area, cm^2
c_p	specific heat capacity at constant pressure, J/(kg·K)
Da	Darcy number, dimensionless
D	diffusion coefficient, m^2/s
d_p	electrode particle diameter, m
E	reversible electrochemical cell voltage, V
E_a	activation energy, kJ/mol,
F	Faraday constant, 96485 C/mol
F_{ij}	view factor, dimensionless
$h_{s,g}$	heat transfer coefficient, $W/(m^2 \cdot K)$
h_v	volume heat transfer coefficient, $W/(m^3 \cdot K)$
i	current density, A/cm^2
i_0	exchange current density, A/cm^2
k	thermal conductivity, W/(m·K)
k_i	reaction rate constant, $mol/(m^3 \cdot Pa^2 \cdot s)$
k'	Boltzmann's constant, J/K
k''	pre-exponential factor, $1/(\Omega \cdot m^2)$
K_e	equilibrium constant, Pa^2 or dimensionless
l_{TPB}	length of the three-phase boundary, m
M_i	molecular weight of species i, kg/mol
n_e	number of electrons transferred per reaction, dimensionless

Nu	Nusselt number, dimensionless
p	pressure, Pa, bar
q	heat flux, W/m^2
Q	source term (heat), W/m^3
r_i	chemical reaction rate, $mol/(m^3 \cdot s)$, $mol/(m^2 \cdot s)$
r'	average pore radius, m
R	gas constant, 8.314 J/(mol·K)
SA	surface area ratio, m^2/m^3
S_i	source term mass, $kg/(m^3 \cdot s)$
T	temperature, K
$\mathbf{T}$	viscous stress tensor, N/m^2
t	tortuosity, dimensionless
u,v	velocity, m/s
w_i	mass fraction of species i, kg/kg
x_j	molar fraction of species j, mol/mol

Greek symbols

α	absorptivity, m^2/mol
ε	emissivity, dimensionless
φ	porosity, dimensionless
η	over potential, V
κ	permeability, m^2
κ_{dv}	deviation from thermodynamic equilibrium, Pa·s
μ	dynamic viscosity, Pa·s
ρ	density, kg/m^3
σ	ionic/electronic conductivity, $\Omega^{-1}m^{-1}$
ø	charge potential

Subscripts

a	anode
act	activation polarization
c	cathode
e	electrode, $e \in \{a,c\}$
el	electrolyte, electrons
eff	effective
f	fluid phase
g	gas phase
i	molecule i
io	ions
j	molecule j
K	Knudsen diffusion
r	steam reforming reaction
por	porous media
s	solid phase, water-gas shift reaction, catalytic site

Abbreviations

CFD	computational fluid dynamics
CM	continuum methods
DFT	density functional theory
DGM	dusty-gas model
FC	fuel cell
FEM	finite element method
FM	Fick's model
FVM	finite volume method
HCR	heterogeneous reaction mechanism
HT	high temperature
IEA	International Energy Agency
IT	intermediate temperature
LBM	Lattice-Boltzmann method

LSM	strontium doped lanthanium manganite
LTE	local temperature equilibrium
LTNE	local temperature non-equilibrium
MC	Monte Carlo
MD	molecular dynamics
PWC	point wise coupling methodology
SA	surface area
SMM	Stefan-Maxwell model
SOFC	solid oxide fuel cell
TPB	three-phase boundary
YSZ	yttria-stabilized zirconia

Chemical

CH_4	methane
CO	carbon monoxide
CO_2	carbon dioxide
e^-	electron
H_2	hydrogen
H_2O	water
N_2	nitrogen
NH_3	ammonia
Ni	nickel
O_0^X	lattice oxygen
O_2	oxygen
OH^-	hydroxyl ion
$V_0^{\cdot\cdot}$	oxygen vacancy

7 Acknowledgement

The Swedish Research Council (VR) and the European Research Council (ERC) support the current research.

8 References

[1] P.-W. Li, L. Schaefer, M.K Chyu, Multiple Transport Processes in Solid Oxide Fuel Cells, Chapter 1 in B. Sundén, M. Faghri (Eds.), Transport Phenomena in Fuel Cells, WIT Press, UK, 2005.

[2] J. Yuan, M. Faghri, B. Sundén, On Heat and Mass Transfer Phenomena in PEMFC and SOFC and Modelling Approaches, Chapter 4 in B. Sundén, M. Faghri (Eds.), Transport Phenomena in Fuel Cells, WIT Press, UK, 2005.

[3] Fuel Cell Handbook (the seventh edition), EG&G Technical Services Inc., U.S. Department of Energy, Morgantown, Virginia, USA, 2004.

[4] S. Kackac, A. Pramuanjaroenkij, X. Zhou, A Review of Numerical Modeling of Solid Oxide Fuel Cells, I. J. Hydrogen Energy 32 (2007) 761-786.

[5] B. Zhu, Next generation fuel cell R&D, Int. J. Energy Res. 30 (2006) 895-903.

[6] M. Ni, D.Y.C. Leung, M.K.H. Leung, Modeling of Methane Fed Solid Oxide Fuel Cells: Comparison Between Proton Conducting Electrolyte and Oxygen Ion Conducting Electrolyte, J. Power Sources 183 (2008) 133-142.

[7] M. Saxe, Bringing Fuel Cells to Reality and Reality to Fuel Cells, Doctoral Thesis, Department of Chemical Sciences and Engineering, KTH- Royal Institute of Technology, Sweden, 2008.

[8] M. Kemm, Dynamic Solid Oxide Fuel Cell Modelling for Non-steady State Simulation of System Applications, Doctoral Thesis, Department of Energy Sciences, Lund University, Sweden, 2006.

[9] H. Zhu, R. Kee, V. Janardhanan, O. Deutschmann, D. Goodwin, Modeling Elementary Heterogeneous Chemistry and Electrochemistry in Solid-Oxide Fuel Cells, J. Electrochem. Soc. 152 (2005) A2427-A2440.

[10] M. Ni, M.K.H. Leung, D.Y.C Leung, Ammonia-Fed Solid Oxide Fuel Cells for Power Generation – A Review, Int. J. Energy Res. 33 (2009) 943-959.

[11] J.B. Gooenough, Y. Huang, Alternative Anode Materials for Solid Oxide Fuel Cells, J. Power Sources 173 (2007) 1-10.

[12] M. Ni, M.K.H. Leung, D.Y.C. Leung, Micro-Scale Modeling of Solid Oxide Fuel Cells with Micro-structurally Grades Electrodes, J. Power Sources 168 (2007) 369-378.

[13] F.Calise, G. Feruzzi, L. Vanoli, Parametric Exergy Analysis of a Tubular Solid Oxide Fuel Cell (SOFC) Stack through Finite-Volume Model, Applied Energy 86 (2009) 2401-2410.

[14] M. Santin, A. Traverso, L. Magistri, Liquid Fuel Utilization in SOFC Hybrid Systems, Applied Energy 86 (2009) 2204-2212.

[15] J. Yuan, B. Sundén, Analysis of Chemically Reacting Transport Phenomena in an Anode Duct of Intermediate Temperature SOFCs, J. Fuel Cell Sci. Technol. 3 (2006) 687-701.

[16] N.J. Hyun, J.D. Hyup, A Comprehensive Micro-scale Model for Transport and Reaction in Intermediate Temperature Solid Oxide Fuel Cells, Electrochim. Acta 51 (2006) 3446-3460.

[17] M.M. Hussain, X. Li, I. Dincer, Mathematical Modeling of Transport Phenomena in Porous SOFC Anodes, Int. J. Thermal Sciences 46 (2007) 48-86.

[18] J. Yuan, Y. Huang, B. Sundén, W.G. Wang, Analysis of Parameter Effects on Chemical Coupled Transport Phenomena in SOFC Anodes, Heat Mass Transfer 45 (2009) 471-484.

[19] R. Suwanwarangkul, E. Croiset, M.W. Fowler, P.L. Douglas, E. Entchev, M.A. Douglas, Performance Comparison of Fick's, Dusty-gas and Stefan-Maxwell Models to Predict the Concentration Overpotential of a SOFC Anode, J. Power Sources 122 (2003) 9-18.

[20] B.A. Haberman, J.B. Young, Three-Dimensional Simulation of Chemically Reacting Gas Flows in the Porous Support Structure of an Integrated-Planar Solid Oxide Fuel Cell, Int. J. Heat and Mass Transfer 47 (2004) 3617-3629.

[21] J.R. Ferguson, J.M. Fiard, R. Herbin, Three-dimensional Numerical Simulation for Various Geometries of Solid Oxide Fuel Cells. J. Power Sources 58 (1996) 109-122.

[22] K. Tseronis, I. Kookos, K. Theodoropoulos, Modelling Mass Transport in Solid Oxide Fuel Cell Anodes: A Case for a Multidimensional Dusty Gas-Based Model, Chem. Eng. Sci. 63 (2008) 5626-5638.

[23] W. Lehnert, J. Meusinger, F. Thom, Modelling of Gas Transport Phenomena in SOFC Anodes, J. Power Sources 87 (2000) 57-63.

[24] H. Yakabe, M. Hisinuma, M. Uratani, Y. Matsuzaki, I. Yasuda, Evaluation and Modeling of Performance of Anode-Supported Solid Oxide Fuel Cell, J. Power Sources 86 (2000) 423-431.

[25] R. Bove, S. Ubertini, Modeling Solid Oxide Fuel Cell Operation: Approaches, Techniques and Results, J. Power Sources 159 (2006) 543-559.

[26] A. Pramuanjaroenkij, S. Kakac, X.Y. Zhou, Mathematical Analysis of Planar Solid Oxide Fuel Cells, Int. J. Hydrogen Energy 33 (2008) 2547-2565.

[27] V. Janardhanan, O. Deutschmann, CFD Analysis of a Solid Oxide Fuel Cell with Internal Reforming, J. Power Sources 162 (2006) 1192-1202.

[28] P. Ivanov, Thermodynamic Modeling of the Power Plant Based on the SOFC with Internal Steam Reforming of Methane, Electrochem. Acta 52 (2007) 3921-3928.

[29] W.Y. Lee, D. Wee, A.F. Ghoniem, An Improved One-Dimensional Membrane-Electrolyte Assembly Model to Predict the Performance of Solid Oxide Fuel Cell Including the Limiting Current Density, J. Power Sources 186 (2009) 417-427.

[30] S.H. Chan, K.A. Khor, Z.T. Xia, A Complete Polarization Model of a Solid Oxide Fuel Cell and its Sensitivity to Change of Cell Component Thickness, J. Power Sources 93 (2001) 130-140.

[31] M. Ni, M.K.H. Leung, D.Y.C. Leung, Micro-Scale Modeling of a Functionally Graded Ni-YSZ Anode, Chem. Eng. Technol. 30 (2007) 287-592.

[32] COMSOL Multiphysics 3.5 user guide, Stockholm, Sweden, 2008.

[33] M. Andersson, Modeling and Simulation for Anode-Supported SOFCs, Licentiate Thesis, Department of Energy Sciences, Lund University, 2009.

[34] W. Bi, D. Chen, Z. Lin, A Key Geometric Parameter for the Flow Uniformity in Planar Solid Oxide Fuel Cell Stacks, Int. J. Hydrogen Energy 34 (2009) 3873-3884.

[35] M. Le Bars, M. Grae Worster, Interfacial Conditions Between a Pure Fluid and a Porous Medium, Implications for Binary Alloy Solidification, J. Fluid Mech. 550 (2006) 149-173.

[36] H.K. Versteeg, W. Malalasekera, An Introduction to Computational Fluid Dynamics, The Finite Volume Method, Pearson, UK, 1995.

[37] W.G. Bessler, S. Gewies, M. Vogler, A New Framework for Physically Based Modeling of Solid Oxide Fuel Cells, Electrochem. Acta 53, (2007) 1782-1800.

[38] S. Lister, N. Djilali, Two-Phase Transport in Porous Gas Diffusion Electrodes, Chapter 5 in B. Sundén, M. Faghri (Eds.), Transport Phenomena in Fuel Cells, WIT Press, UK, 2005.

[39] M. Boder, R. Dittmeyer, Catalytic Modification of Conventional SOFC Anodes with a View to Reducing Their Activity for Direct Internal Reforming of Naturalgas, J. Power Sources 155 (2006) 13-22.

[40] D.L. Damm, A.G. Fedorov, Local Thermal Non-Equilibrium Effects in Porous Electrodes of the Hydrogen Fueled SOFC, J. Power Sources 159 (2006) 1153-1157.

[41] C.H. Chao, A.J.J. Hwang, Predictions of Phase Temperatures in a Porous Cathode of Polymer Electrolyte Fuel Cells using a Two-Equation Model, J. Power Sources 160 (2006) 1122-1130.

[42] I. Dincer, F. Hamdullahpur, A Review on Macro-Level Modeling of Planar Oxide Fuel Cells, Int. J. Energy Res. 32 (2008) 336-355.

[43] S.M. Haile, Fuel Cell Materials and Components, Acta Mater. 51 (2003) 1981-2000.

[44] M. Vogler, A. Bieberle-Hütter, L. Gauckler, J. Warnatz, W.G. Bessler, Modelling Study of Surface Reactions, Diffusion, and Spillover at a Ni/YSZ Patterned Anode, J. Electrochem. Soc. 156 (2009) B663-B672.

[45] V.M. Janardhanan, V. Heuveline, O. Deutschmann, Three-Phase Boundary Length in Solid-Oxide Fuel Cells: A Mathematical Model, J. Power Sources 178 (2008) 368-372.

[46] P. Asinari, M.C. Quaglia, M.R. von Sakovsky, B.V. Kasula, Direct Numerical Calculation of the Kinematic Tortuosity of Reactive Mixture Flow in the Anode Layer of Solid Oxide Fuel Cells by Lattice Boltzmann Method, J. Power Sources 170 (2007) 359-375.

[47] A.S. Martinez, J. Brouwer, Percolating Modeling Investigation of TPB Formation in a Solid Oxide Fuel Cell Electrode-Electrolyte Interface, Electochem. Acta 53 (2008) 3597-3609.

[48] V.M. Janardhanan, O. Deutschmann, Numerical Study of Mass and Heat Transport in Solid-Oxide Fuel Cells Running on Humidified Methane, Chem. Eng. Sci. 62 (2007) 5473-5486.

[49] Y.M. Barzi, M. Ghassemi, M.H. Hamedi, E. Afshari, Numerical Analysis of Output Characteristics of a Tubular SOFC with Different Fuel Compositions and Mass Flow Rates. In: Proceedings of Solid Oxide Fuel Cells 10 (SOFCX), K. Eguchi, S.C. Singhal, H. Yokokawa, J. Mizusaki (Eds.), ECS Transactions 7 (2007) 1919-1928.

[50] S. Clarke, A. Dicks, K. Pointon, T. Smith, A. Swann, Catalytic Aspects of the Steam Reforming of Hydrocarbons in Internal Reforming Fuel Cells, Catalysis Today 38 (1997) 411-423.

[51] P. Aguiar, C.S. Adjiman, N.P. Brandon, Anode-Supported Intermediate-Temperature Direct Internal Reforming Solid Oxide Fuel Cell II. Model-Based Dynamic Performance and Control, J. Power Sources 147 (2005) 136-147.

[52] D. Sanchez, R. Chacartegui, A. Munoz, T. Sanchez, On the Effect of Methane Internal Reforming Modeling in Solid Oxide Fuel Cells, Int J. Hydrogen Energy 33 (2008) 1834-1844.

[53] J.-M. Klein, Y. Bultel, S. Georges, M. Pons, Modeling of a SOFC Fuelled by Methane: From Direct Internal Reforming of Gradual Internal Reforming, Chem. Eng. Sci. 62 (2007) 1636-1649.

[54] F. Nagel, T. Schildhauer, S. Biollaz, S. Stucki, Charge, Mass and Heat Transfer Interactions in Solid Oxide Fuel Cells Operated with Different Fuel Gases – A Sensitivity Analysis, J. Power Sources 184 (2008) 129-142.

[55] L. Wang, H. Zhang, S. Weng, Modeling and Simulation of Solid Oxide Fuel Cell Based on the Volume-Resistance Characteristic Modeling Technique, J. Power Sources 177 (2009) 579-589.

[56] J.-M. Klein, Y. Bultel, M. Pons, P. Ozil, Current and Voltage Distributions in a Tubular Solid Oxide Fuel Cell (SOFC), J. Applied Electrochemistry 38 (2008) 497-505.

[57] P. Aguiar, C.S. Adjiman, N.P. Brandon, Anode-Supported Intermediate Temperature Direct Internal Reforming Solid Oxide Fuel Cell. I: Model-Based Steady-State Performance, J. Power Sources 138 (2004) 120-136.

[58] P. Hofmann, K.D. Panopoulos L.E. Fryda, E. Kakaras, Comparison between Two Methane Reforming Models Applied to a Quasi-Two-Dimensional Planar Solid Oxide Fuel Cell Model, Energy (2008) 1-7.

[59] D. King, J. Strohm, X. Wang, H.-S. Roh, C. Wang, Y.-H. Chin, Y. Wang, Y. Lin, R. Rozmiarek, P. Singh, Effect on Nickel Microstructure on Methane Steam Reforming Activity of Ni-YSZ Cermet Anode Catalyst, J. Catalysis 258 (2008) 356-365.

[60] B. Sundén, J. Yuan, Development of Multi-scale Models for Transport Processes Involving Catalytic Reactions in SOFCs, Int. J. Micro-nano Scale Transport 1 (2010).

[61] E. Hecht, G. Gupta, H. Zhu, A. Dean, R. Kee, L. Maier, O. Deutschmann, Methane Reforming Kinetics Within a Ni-YSZ SOFC Anode Support, Applied Catalysis A: General 295 (2005) 40-51.

[62] J. Molenda, K. Swierczek, W. Zajac, Functional Materials for IT-SOFC, J. Power Sources 173 (2007) 657-670.

[63] V.M. Janardhanan, O. Deutschmann, CFD Analysis of a Solid Oxide Fuel Cell with Internal Reforming: Coupled Interactions of Transport, Heterogeneous Catalysis and Electrochemical Processes, J. Power Sources 162 (2006) 1192-1202.

[64] T. Karakasidis, C. Charitidis, Multiscale Modelling in Nanomaterials Scince, Mater. Sci. Eng. C27 (2007) 1082-1089.

[65] C. Frayret, A. Villesuzanne, M. Pouchard , S. Matar, Density Functional Theory Calculations on Microscopic Aspects of Oxygen Diffusion in Ceria-Based Materials, I. J. Quantum Chemistry 101 (2005) 826-839.

[66] C.H. Cheng, Y.W. Chang, C.W. Hong, Multiscale Parametric Studies on the Transport Phenomenon of a Solid Oxide Fuel Cell, J. Fuel Cell Sci. Technol. 2 (2005) 219-225.

[67] A.U. Modak, M.T. Lusk, Kinetic Monte Carlo Simulation of a Solid-Oxide Fuel Cell, Solid State Ionics 176 (2005) 1281-1291.

[68] A.S. Joshi, K.N. Grew, A.A. Peracchio, W.K.S. Chiu, Lattice Boltzmann Modeling of 2D Gas Transport in a Solid Oxide Fuel Cell Anode, J. Power Sources 164 (2007) 631-638.

[69] W. Huang, X. Huang, K. Reifsnider, Meso-Scale Multhiphysics Model of SOFC Cathode Processes, COMSOL Users Conference Boston, 2006.

[70] U. Pasaogullari, C.-Y. Wang, Computational Fluid Dynamics Modeling of Solid Oxide Fuel Cells, S.C. Singhal and M. Dokiya (Eds.), Proceedings of SOFC-VIII (2003) 1403-1412.

[71] N. Autissier, D. Larrain, J. van Herle, D. Favrat, CFD Simulation Tool for Solid Oxide Fuel Cells, J. Power Sources 131 (2004) 131-139.

[72] M.A. Khaleel, D.R. Rector, Z. Lin, K. Johnson, K. Recknagle, Multiscale Electrochemistry Modeling of Solid Oxide Fuel Cells, Int. J. Multiscale Comp. Eng. 3 (2005) 33-47.

[73] B.H. Dennis, Z. Han, W. Jin, B.P. Wang, L. Xu, T. Aapro, A. Ptchelintsev, T. Reinikainen, Multi-Physics Simulation Strategies with Application to Fuel Cell Modeling, 7th. Int. Conf. on Thermal, Mechanical and Multiphysics Simulation and Experiments in Micro-Electronics and Micro-Systems, EuroSimE, 2006.

[74] N. Asproulis, M. Kalweit, D. Drikakis, Hybrid Molecular-Continuum Methods for Micro- and Nanoscale Liquid Flows, 2nd Micro and Nano Flows Conference West London, UK, 2009

[75] K. Reifsnider, X. Huang, G. Ju, R. Solasi, Multi-Scale Modeling Approaches for Functional Nano-composite Materials, J. Mater. Sci. 41 (2006) 6751-6759.

[76] R. Bove, P. Lunghi, N.M. Sammes, SOFC Mathematical Model for Systems Simulation. Part One: From a Micro-Detailed to Macro-Black-Box Model, Int. J. Hydrogen Energy 30 (2005) 181-187.

[77] K. Haraldsson, K. Wipke, Evaluating PEM Fuel Cell System Models, J. Power Sources 126 (2004) 55-97.

[78] A. Faghri, Z. Guo, Challenges and Opportunities of Thermal Management Issues Related to Fuel Cell Technology and Modeling, Int. J. Heat and Mass Transfer 48 (2005) 3891-3920.

[79] J. Park, X. Li, Multi-Phase Micro-Scale Flow Simulation in the Electrodes of a PEM Fuel Cell by Lattice Boltzmann Method, J. Power Sources 178 (2008) 248-257.

[80] C. Nicotella, A. Bertei, M. Viviani, A. Barbucci, Morphology and Electrochemical Activity of SOFC Composite Cathodes: II. Mathematical Modeling, J Appl. Electrochem. 39 (2009) 503-511.

[81] M. Peksen, R. Peters, L. Blum, D. Stolten, Numerical Modeling and Experimental Validation of a Planar Type Pre-Reformer in SOFC Technology, Int. J. Hydrogen Energy 34 (2009) 6425-6436.

[82] K. Tseronis, I. Kookos, K. Theodoropoulos, Modelling and Design of the Solid Oxide Fuel Cell Anode, COMSOL Users Conference Birmingham, 2006.

[83] S.H. Chan, C.F. Low, O.L. Ding, Energy and Exergy Analysis of Simple Solid-Oxide Fuel-Cell Power Systems, J. Power Sources 103 (2002) 188-200.